Analysis of Membrane Fusion as a Two-State Sequential Process: Evaluation of the Stalk Model

Gabriel Weinreb† and Barry R. Lentz*
*Departments of Biochemistry and Biophysics, and †Cell and Developmental Biology, University of North Carolina at Chapel Hill, Chapel Hill, North Carolina

ABSTRACT We propose a model that accounts for the time courses of PEG-induced fusion of membrane vesicles of varying lipid compositions and sizes. The model assumes that fusion proceeds from an initial, aggregated vesicle state ((A) membrane contact) through two sequential intermediate states (I_1 and I_2) and then on to a fusion pore state (FP). Using this model, we interpreted data on the fusion of seven different vesicle systems. We found that the initial aggregated state involved no lipid or content mixing but did produce leakage. The final state (FP) was not leaky. Lipid mixing normally dominated the first intermediate state (I_1), but content mixing signal was also observed in this state for most systems. The second intermediate state (I_2) exhibited both lipid and content mixing signals and leakage, and was sometimes the only leaky state. In some systems, the first and second intermediates were indistinguishable and converted directly to the FP state. Having also tested a parallel, two-intermediate model subject to different assumptions about the nature of the intermediates, we conclude that a sequential, two-intermediate model is the simplest model sufficient to describe PEG-mediated fusion in all vesicle systems studied. We conclude as well that a fusion intermediate "state" should not be thought of as a fixed structure (e.g., "stalk" or "transmembrane contact") of uniform properties. Rather, a fusion "state" describes an ensemble of similar structures that can have different mechanical properties. Thus, a "state" can have varying probabilities of having a given functional property such as content mixing, lipid mixing, or leakage. Our data show that the content mixing signal may occur through two processes, one correlated and one not correlated with leakage. Finally, we consider the implications of our results in terms of the "modified stalk" hypothesis for the mechanism of lipid pore formation. We conclude that our results not only support this hypothesis but also provide a means of analyzing fusion time courses so as to test it and gauge the mechanism of action of fusion proteins in the context of the lipidic hypothesis of fusion.

INTRODUCTION

Membrane fusion plays essential roles in all cells, being critical to such processes as cellular trafficking, intercellular communication, and sexual reproduction. It also plays a critical role in the life cycle of several deadly viruses such as HIV, influenza, and Ebola. Although considerable effort has been devoted to studying fusion in both model and biomembranes, the physical basis of this phenomenon is still not completely understood. Most models of the fusion process assume a sequence of events leading from contacted membranes to fusion product. Even though fusion in vivo is catalyzed by fusion proteins, it clearly involves rearrangements of lipid structures and is sensitive to lipid composition (1). Many efforts to define these lipid rearrangements are based on the so-called ''stalk'' model (2–4). The ''stalk'' is viewed as a highly distorted lipid arrangement more akin to nonlamellar than to lamellar (i.e., membrane-like) lipid phases. In this structure, contacting monolayers are merged but *trans*-monolayers remain intact and separate the two aqueous compartments. A second type of intermediate structure, the ''modified stalk'' or ''transmembrane contact'' (TMC) is described as possibly having a lower energy than the stalk (5). In this structure, the stalk expands radially so that *trans*-monolayers come into contact at their hydrophobic surfaces to form a small bilayer between aqueous compartments. We recently calculated, using a macroscopic materials approach, the free energy for evolution of fusion intermediates as a function of the stalk radius and found free energy minima near the stalk and TMC structures (6). A similar result was obtained using Monte Carlo simulation of short copolymers designed to mimic lipids in bilayer and evolving stalk arrangements (7). Both results imply two semistable intermediates on the path from contacting membranes to a fusion pore.

Experimental evidence for two intermediates derives from our studies of poly (ethylene glycol) (PEG)-mediated fusion between 45 nm vesicles (8). A rapidly formed, reversible intermediate produced lipid mixing and unstable pore formation, whereas the second intermediate formed more slowly

Submitted May 24, 2006, and accepted for publication February 2, 2007.

Address reprint requests to Barry R. Lentz, E-mail: uncbrl@med.unc.edu.

Abbreviations used: TMC, transmembrane contact; CH, cholesterol; DOPC, 1,2-dioleoyl-3-*sn*-phosphatidylcholine; DC18:3PC, 1,2-dilinolenoyl-*sn*-phosphatidylcholine; DLPC, dilauroylphosphatidylcholine; DOPE, 1,2-dioleoyl-3-*sn*-phosphatidylethanolamine; SM, sphingomyelin; β-BODIPY530/550 C_{12}-HPE, 2-(4,4-difluoro-5,7-diphenyl-4-bora-3a,4a-diaza-*s*-indacene-3-dodecanoyl)-1-hexadecanoyl-*sn*-glycero-3-phosphoethanolamine; β-BODIPY500/510 C_{12}-HPC, 2-(4,4-difluoro-5,7-diphenyl-4-bora-3a,4a-diaza-*s*-indacene-3-dodecanoyl)-1-hexadecanoyl-*sn*-glycero-phosphocholine; DPA, dipicolinic acid; TES, *N*-[tris(hydroxymethyl)methyl]-2-aminoethanesulfonic acid; PEG, poly(ethylene glycol); $C_{12}E_8$, dodecyloctaethylene glycol monoether; PY-Ch, cholesteryl 1-pyrenebutyrate; DOPS, dioleoylphosphatidylserine; Tris, tris(hydroxymethyl)aminomethane; LM, lipid mixing; CM, content mixing; E/M, excimer/monomer fluorescence intensity ratio; FRET, fluorescence resonance energy transfer.

0006-3495/07/06/4012/18 $2.00

doi: 10.1529/biophysj.106.090043

and was committed to proceed to a stable fusion pore (8). These observations provided direct experimental evidence, at least for lipid vesicles of one size and composition, for a sequential mechanism proceeding through more than one intermediate. Fusion of lipid vesicles with a planar bilayer was also observed to proceed through an initial lipid-mixed intermediate in which flickering pores were noted (9), in agreement with our studies of 45 nm vesicle fusion. Observations on PEG-mediated fusion between either 20–23 nm or 110–125 nm vesicles produced from the same lipid mixture did not show two distinct steps as seen for the 45 nm vesicles, but rather revealed a process described by two exponentials in time. We have also observed that lipid composition (10,11), membrane curvature (11), the presence of higher concentrations of PEG (12), or the presence of transmembrane protein domains (13) or fusion peptides (10) all influence whether one or two exponentials are observed in the time course of fusion pore formation. Although we have interpreted the appearance of two exponentials in terms of a multistep process (12), this is qualitative and does not establish a particular kinetic model within which to interpret preexponential factors or exponential constants in terms of specific events in the process.

In this article, we test quantitatively a sequential mechanism suggested by these calculations and observations. In this model (see Fig. 1), a state of membrane close contact (A, aggregated state) proceeds to an initial intermediate (I_1, ostensibly but not necessarily the stalk) in which some membrane components mix (lipids or proteins) and which can support limited and perhaps transient pore formation. This intermediate is assumed here to form irreversibly, an assumption supported by analysis of reversible observables. The initial intermediate converts to the second intermediate (I_2) that then converts to a stable fusion pore (FP) in an irreversible fashion. In devising this quantitative test of the sequential model for fusion, we sought to answer the following questions:

1. Can a sequential model explain the time courses of various measured events during PEG-mediated fusion? If so, how many intermediate states are required to describe the observations?
2. What are the experimental observations necessary to define the kinetic and physical characteristics of the states identified in the simplest model?
3. Does the success of the sequential model offer support for the ''modified stalk'' hypothesis for the mechanism of lipidic pore formation during fusion?
4. Does the model allow us to extract information related to functional properties of the fusion intermediate states?

EXPERIMENTAL PROCEDURES

Materials

Chloroform stock solutions of 1,2-dioleoyl-3-*sn*-phosphatidylcholine (DOPC), 1,2-dioleoyl-3-*sn*-phosphatidylethanolamine (DOPE), and sphingomyelin (SM) (bovine brain) were purchased from Avanti Polar Lipids (Birmingham, AL) and used without further purification. The concentrations of all the stock lipids were determined by phosphate assay (14). Cholesterol (CH) was purchased from Avanti Polar Lipids and was further purified as previously reported (15). 2-(4,4-Difluoro-5,7-diphenyl-4-bora-3a,4a-diaza-*s*-indacene-3-dodecanoyl)-1-hexadecanoyl-*sn*-glycero-3-phosphoethanolamine (β-BODIPY530/550 C_{12}-components HPE), 2-(4,4-difluoro-5,7-diphenyl-4-bora-3a,4a-diaza-*s*-indacene-3-dodecanoyl)-1-hexadecanoyl-*sn*-glycero-phosphocholine (β-BODIPY500/510 C_{12}-HPC), and cholesteryl 1-pyrenebutyrate (pyrene cholesterol; PY-Ch) were purchased from Molecular Probes (Eugene, OR). Terbium (Tb^{3+}) chloride was purchased from Johnson Matthey (Ward Hill, MA). Dipicolinic acid (DPA) and *N*-[tris(hydroxymethyl)methyl]-2-aminoethanesulfonic acid (TES) were purchased from Sigma Chemical (St. Louis, MO). Poly(ethylene glycol) of molecular weight 7000–9000 (PEG 8000) was purchased from Fisher Scientific (Fairlane, NJ) and further purified as previously reported (16). Dodecyloctaethylene glycol monoether ($C_{12}E_8$) was purchased from Calbiochem (La Jolla, CA). All other reagents were of the highest purity grade available.

Vesicle preparation was carried out as described previously (10,17,18), with vesicle size determined by quasielastic light scattering (19). A solid particle model was used to analyze correlation functions for 20–25 nm vesicles, whereas a shell model was used for 110–125 nm vesicles.

Content mixing and leakage were followed using the Tb^{3+}/DPA content mixing and leakage assays based on those originally proposed by (20) and modified for our purposes (21). Fluorescence was monitored with a SLM-48000MHF Spectrofluorometer (SLM Aminco, Urbana, IL), with excitation at 278 nm and emission read at 545 nm. Even though ''percent of content mixing and leakage'' (see Talbot et al. (21) for details) are measures of the fusogenic potential of a given vesicle system, we do not concern ourselves here with these quantities but rather with the kinetics of how these events evolve during fusion and with the normalized probabilities that they appear in the different states of our sequential kinetic model. The maximal percent content mixing for each system is nonetheless given for each system for the sake of comparison with previous reports.

Lipid mixing

Fluorescent lipid probes with fluorophores attached to their acyl-chains, BODIPY500-PC, and BODIPY530-PE were used as described previously for measuring lipid mixing during PEG-mediated vesicle fusion (22). The fluorescence readout from this assay can be compared to the fluorescence of vesicles following addition of detergent (taken as 100% lipid mixing) to obtain ''% lipid mixing''. This is a measure of size of PEG-induced aggregates and the number of productive (i.e., membrane-joining) contacts within aggregates (8,12). Again, we do not concern ourselves with this quantity, but the maximum % lipid mixing associated with each vesicle system is still given for reference. Note that the context mixing, leakage, and lipid mixing measurements reflect diffusion processes that are irreversible. This is important to keep in mind when modeling the observations. Even though individual events may be reversible, the observations are cumulative.

Inner leaflet lipid mixing

This assay uses [*N*-(7-nitro-2,1,3-benzoxadiazol-4-yl)-1,2-dioleoyl-3-*sn*-phosphatidylserine] (NBD-PS) incorporated at self-quenching concentrations (lipid/probe = 10:1) (23). NBD-PS exposed in the outer leaflet is reduced with sodium dithionite and the change in NBD fluorescence lifetime upon dilution of probe into fused vesicle partners gives a direct measure of the dilution factor. Comparison of the observed dilution factor to that expected for complete fusion gives the percent inner leaflet mixing (23).

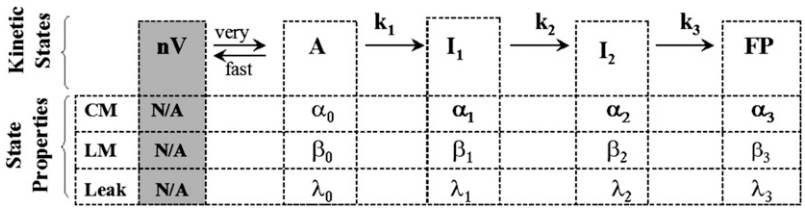

FIGURE 1 Schematic of the sequential two-intermediate-state model for fusion considered here. ''nV'' is a state consisting of separate vesicles; ''A'' is a state with vesicles in contact within aggregates; I_1 and I_2 are intermediate states (perhaps frequently discussed ''stalk'' and ''TMC'' (4,5,27); and FP is the final fusion pore state. Each state is characterized by the probability of observing ''fusion events'' (content mixing $\{\alpha_i\}$, lipid mixing $\{\beta_i\}$), and by a content leakage rate (λ_i). Three rate constants (k_i) are also required to define the model. After fixing experimentally defined parameter values and applying normalization conditions, the model is defined by nine parameters (four probabilities, two leakage rates, and three rate constants).

Light scattering

Light scattering was measured at a right angle to incident light on a spectrofluorometer (SLM 48000MHF, SLM Aminco, Urbana, IL) using the same settings as for the content mixing and leakage assays.

Fusion intermediate detection

The local concentration of PY-CH rises and then drops during fusion, as indicated by formation of pyrene excited-state complexes (excimers), detected by the ratio of fluorescence intensity of the excimer to that of the monomer (E/M ratio) (17). Comparison of this behavior with that observed for pyrene cholesterol fluorescence during the lamellar-to-hexagonal phase transition suggests the presence of nonlamellar structures during the fusion process (17).

MODEL DEVELOPMENT AND COMPUTATIONAL PROCEDURES

The model

The description of our model for membrane fusion is organized around four issues (Fig. 1): i), aggregation and fusible complex formation; ii), meaning of intermediate fusion ''states''; iii), evolution of kinetic states leading to fusion: sequential versus parallel models; and iv), linkage of the properties of kinetic states to the observables (lipid and content mixing, leakage, etc.).

Aggregation and fusible complex formation

In our experimental procedure, aggregation and close contact between vesicles is accomplished by means of a low concentration of PEG. PEG has two effects: first, it brings bilayers reversibly into close contact (24); second, the compressive osmotic stress created by PEG promotes evolution from the initial intermediate to the pore (6,18). Lipid mixing between nonfusing vesicles becomes complete only after multiple aggregation/disaggregation cycles (25), indicating that aggregate sizes are finite. Measurements of the size of vesicles resulting from PEG-mediated fusion confirm that aggregation numbers (N) range from just five or six for 45 nm (8) vesicles to between 10 and 20 for 20–23 nm vesicles (12) and that the extent of lipid mixing is related to the aggregation number (26). Thus, aggregate size limits the number of productive intermembrane contacts leading to lipid mixing and fusion. In addition, the distance of membrane-membrane approach is crucial to fusion (24), and this distance will vary depending on geometric restraints related both to the packing of vesicles within an aggregate and to the osmotic pressure compressing the aggregate (i.e., the PEG concentration). Thus, we assume that the final level of lipid mixing reflects both the size of aggregates and the number of productive contacts in the aggregated state. Our lipid mixing assay produces an increase in fluorescence proportional to the extent of probe dilution from probe-rich into probe-free vesicles (22). Thus, the fraction of lipid mixing ($F_{LM}(t)$) is just the ratio of the dilution factor measured at time t (L/P) to that expected for complete dilution (n) of probe-containing vesicles into probe-free vesicles. We have shown that the dilution factor varies exponentially with the fluorescence signal (either donor/acceptor fluorescence for fluorescence resonance energy transfer assays (22) or fluorescence lifetime for probe self-quenching assays (8)), yielding;

$$F_{LM}(t) = 1/n[\exp k\{F(t) - F(0)\} - 1]. \quad (1a)$$

Thus, one can introduce f_{LM}, the fraction of the maximum possible lipid mixing that occurred in aggregates under a given set of experimental conditions:

$$f_{LM} = \frac{F_{LM}(\infty) - F_{LM}(0)}{F_{LM}(\text{detergent}) - F_{LM}(0)}, \quad (1b)$$

where the numerator reflects the maximal signal that occurred during lipid mixing and the denominator reflects the maximal possible lipid mixing determined after addition of detergent that mixes all lipids in the system completely. As the number of intervesicle productive contacts within aggregates and the aggregate size increase, f_{LM} approaches its maximal possible value, 1.

Meaning of fusion intermediate "states"

We must preface our description of the model to which our efforts led by a discussion of what we mean by a ''fusion intermediate state''. Because we had observed PEG-mediated fusion of 45 nm vesicles to involve at least two intermediate states, we attempted to fit various observations with a model that assumed that these were the classical ''stalk'' (27) and transmembrane contact (TMC) (5) structures. As generally pictured and discussed, these structures are considered to permit contacting leaflet mixing but not

content mixing, which is in accordance with the classical ''stalk model''. These are generally described as ''hemifusion'' intermediates in that they do not join membrane-enclosed spaces. Very early on, we determined that it was not possible to describe in this way the many observations we had made on a variety of fusing model membrane systems. Experimentally, only one system behaved in this way (i.e., lipid mixing clearly preceding content mixing), whereas most involved lipid mixing, content mixing, and leakage to varying extents throughout the fusion process. We had to conclude that the intermediate ''states'' are not fixed structures but ensembles of similar structures all having somewhat different detailed mechanical properties that would allow properties such as lipid mixing, content mixing, or leakage to be observed. For instance, some stalk structures in the ensemble might exist as a classical, nonleaky ''stalk'' structure. Others may have the property of a small conducting pore. Transiently formed small conducting pores have been observed by electrophysiological measurements for both biological (28,29) or pure-lipid (9) fusing systems. These events usually lead to the opening of a large fusion pore (30) but not always (31). These transient or ''flickering'' pores may occur only intermittently before full opening. To study the time course of fusion, one would need to make many single pore observations (i.e., a small ensemble of observations) and average over all of these to obtain the probability that a productive intermembrane contact might have the property of content mixing at any time. Although such an analysis is possible (32,33), it is awkward experimentally and limited in accuracy unless very large numbers of productive contacts (eventual pores) are examined. Alternatively, one can record observations for large numbers of membrane-membrane contacts to obtain an ensemble average. This is our approach and is most convenient in examining the time evolution of a fusing system. This requires that one describe the mechanical properties of a ''fusion state'' as an ensemble average over many similar structures, each having its own particular set of mechanical properties and free energy. (Each ensemble member must be described as open with respect to water, ions, etc., and described by a free energy rather than by an energy.) The observable properties of such a ''state'' must be described by probabilities rather than by fixed values. Thus, the ''fusion intermediate states'' of our model are characterized by probabilities of leaking trapped content and mixing trapped content or lipids between vesicles.

Models considered

The simplest model we considered involved a single intermediate and is described in Appendix I. This model was appropriate to only a very few systems. We reported previously that, even for a fairly simple vesicle system, a model involving two intermediates was required to describe PEG-meditated fusion (8). This led us to consider a sequential, two-intermediate model, as shown in Scheme 2a.

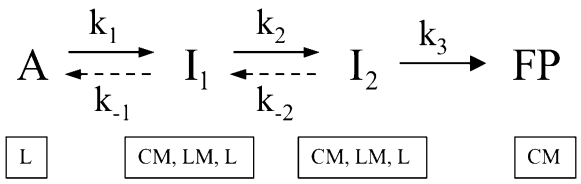

Two-intermediate, sequential model

(2a)

The boxes below each state indicate the possible properties of that state. As mentioned above, intermediate states displayed the properties of leakage (L) and content mixing (CM) as well as the universally accepted property of lipid mixing (LM), but with different probabilities depending on the specific system. The final step in this process (final pore formation) is generally acknowledged to be irreversible. The first two steps are indicated as reversible for the sake of generality, but we have little real information about their reversibility. We know that the first step can reverse if the force maintaining productive contacts is removed (8), but there is no indication that it is reversible if that force is maintained, as in our experiments. Note that the observation of single ''flickering pores'' says nothing about the reversibility of the ensemble I_1 ''state'' that our measurements follow. A single pore that flickers open (microscopic state O) must have a statistical weight close to that of the unopened nascent pore structure (microscopic state U). A thermodynamic state consisting of a mixture of such structures have the property of CM. Experiments suggest that such a state proceeds normally to the FP state in at least one model membrane system even if the aggregating force is removed (8).

For two reasons, we began by assuming that the first two steps are essentially irreversible, i.e., rates of back reactions are insignificant relative to the forward rates. First, this assumption allows a solution with a tractable number of unknown parameters. Second, three of our observables (content leakage and mixing, lipid mixing) involve diffusion, which is an irreversible process. Thus, these measurements cannot provide insights into the nature of reversible steps in the fusion process. If the rates of reverse steps are significant relative to those of forward steps, then the effective forward rate constants that we obtain in this way are complex functions of all rate constants (forward and reverse) up to the final, essentially irreversible step (fusion pore formation, FP state). Note that the number of exponentials describing the kinetics does not depend on whether we assume reversible or irreversible steps, a parallel model, or a sequential model. The number of independent variables determines this number, which, in our case of two intermediates, is three (four states minus one determined from normalization). If we are justified in the assumption of irreversible steps, then the rate constants obtained from fitting the irreversible observations of content mixing, lipid mixing, and leakage are good approximations to the actual forward rates. Measurements based on reversible observables would then also be

well described by these rate constants. We provide evidence in Results under ''Testing model parameters using additional observables'' that this is the case.

We also considered the possibility that the demonstrated two intermediates are located on a parallel pathway, as shown in Scheme 2b.

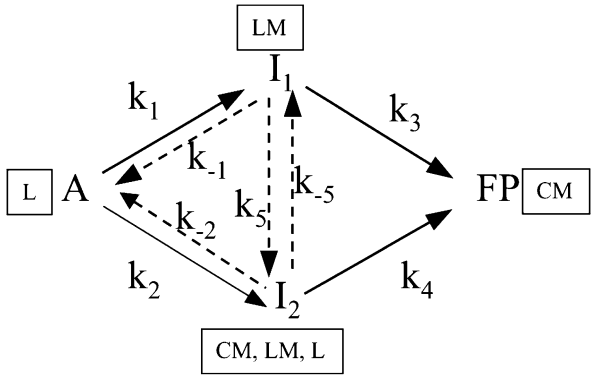

Two-intermediate, parallel stalk model (2b)

Even though this model is much more complex than the sequential model, we considered it to determine if a model that assumed the existence of the commonly envisioned nonleaky stalk structure could account for our observations. Because the stalk ''structure'' (as opposed to ''state'') allows only lipid mixing between juxtaposed monolayers, we placed this requirement on the stalk intermediate in this model. Because content mixing is observed early in the fusion process (in ours and other model systems as well as natural systems), we included a parallel pathway that provided an intermediate ''state'' having the mechanical properties of leakage and content mixing (I_2 in the diagram). Again, we had to make the assumption of irreversibility. To briefly summarize a lengthy testing process, this approach could not describe the data for two reasons. First, we observed two systems with delayed leakage but immediate content mixing. If we allowed I_1 (''stalk'') to display leakage, and demanded that I_2 did not, we could explain this observation with the path $A \rightarrow I_2 \rightarrow I_1 \rightarrow FP$. However, this sequence of events reverts to our sequential model. A second observation is that a single intermediate model best describes some systems. In these instances, this single intermediate must have the property of content mixing. This rules out an initial intermediate having the properties of the classic stalk structure (i.e., no content mixing). Finally, for systems in which two-exponential lipid mixing occurs without leakage, the rate constants defined by lipid mixing invariably also described the two-exponential behavior of content mixing. The parallel two-intermediate stalk model clearly cannot describe this observation, as I_1 in this model does not have the content mixing property. If we relax our assumption and allow I_1 to have content mixing and leakage as properties, this is not the traditional stalk structure, and we revert to a more complex version of the sequential model shown in Scheme 2a. We conclude that the sequential evolution of two irreversible intermediates (Scheme 2a with dashed lines removed) is the simplest model that can explain all the cases of PEG-mediated vesicle fusion that we have studied.

This scheme defines a system of four ordinary differential equations similar to the simpler set of three differential equations shown in Eq. A1. Making the assumption that the first two steps are irreversible leads to the following solution:

$$
\begin{aligned}
A(t) &= e^{-k_1 t},\\
I_1(t) &= \frac{k_1}{k_1 - k_2} \times (e^{-k_2 t} - e^{-k_1 t}),\\
I_2(t) &= -k_1 k_2 \times \left(\frac{e^{-k_1 t}}{[k_1 - k_2][k_3 - k_1]} + \frac{e^{-k_2 t}}{[k_1 - k_2][k_2 - k_3]} \right.\\
&\qquad \left. + \frac{e^{-k_3 t}}{[k_2 - k_3][k_3 - k_1]} \right),\\
FP(t) &= -\frac{k_2 k_3}{[k_1 - k_2][k_3 - k_1]}\left(1 - e^{-k_1 t}\right)\\
&\qquad - \frac{k_1 k_3}{[k_1 - k_2][k_2 - k_3]}\left(1 - e^{-k_2 t}\right)\\
&\qquad - \frac{k_1 k_2}{[k_2 - k_3][k_3 - k_1]}\left(1 - e^{-k_3 t}\right).
\end{aligned}
\tag{3}
$$

Linking model to observable events associated with fusion

All the events that we observe during fusion are recorded as changes in fluorescence signals. Each assay yields a unique signal and has aspects of its treatment that are unique. However, there is a common treatment that relates to all. The total fluorescent signal $F(t)$ originates from the background (F_0) and fluorescent sources in all states. The intensity of fluorescent sources is determined by their number, $N(t)$, in the volume under investigation and the fluorescence F_1 of a single source:

$$F(t) = F_0 + F_1 \cdot N(t). \tag{4}$$

Determination of single source fluorescence, F_1, and the number of these sources, $N(t)$, are generally not practical, but rewriting the expression (Eq. 4) can give us a practical tool to describe the experimental data. Indeed, the maximum change in fluorescence throughout the experiment is proportional to both F_1 and the maximum number (N_{max}) of fluorescent particles in the experimental volume. Therefore the following expression is equivalent to Eq. 4:

$$F(t) = F_0 + \Delta F_\infty \cdot \Phi(t), \tag{4a}$$

where the normalized observable is $\Phi(t) = F_1 \times N(t)/\Delta F_\infty$. This is the ''fractional change'' in the observable, and gives the fraction of the probes that report a fluorescent signal at time t. $\Delta F_\infty = F(\infty) - F_0$ is the maximum signal change for the observable, where $F(\infty)$ is the observed fluorescence

signal at long time (i.e., the asymptotic value). The function $\Phi(t)$ includes two separate processes that take place during fusion: 1), evolution of fusing vesicles through the sequential states presumed by our model for the fusion process; and 2), activation of indicative fluorescence sources (e.g., in the case of content mixing, this is Tb^{3+}-DPA complex formation). Since the second process is caused by diffusion of probe molecules down a concentration gradient, it is expected to be instantaneous on the fusion timescale and inherently irreversible and therefore cumulative. Determination of fractional changes is different for different experiments and will be described in the following sections.

Lipid mixing

The essential assumption we make in relating observable fluorescence signals to the fusion states is that each observable has a defined probability (β_i) that a corresponding signal occurs in a given state *i*. For example, lipid mixing (LM) is detected when BODIPY probes diffuse into probe-free membranes so that fluorescence resonance energy transfer between them becomes insignificant. The probability (β_i) that this occurs in state *i* is related to the rate of probe transfer between contacting vesicles in this state. Although slow lipid transfer occurs between vesicles at PEG concentrations below the fusion threshold (25), the rate increases by 4–5 orders of magnitude at the fusion threshold concentration (34). Such a dramatic increase in rate must correspond to formation of a ''fusion-competent'' state, which is widely seen as the ''stalk'' hemifusion state (I_1), in which contacting membrane monolayers are fused. In this state, probe dilution is limited only by diffusion through the fusion-competent structure, which appears to be very rapid. Probe dilution also occurs when a pore forms and probes in noncontacting monolayers can diffuse into probe-free monolayers. However, this signal is typically insignificant relative to the signal from mixing of contacting monolayers.

The fractional fluorescence change in case of lipid mixing $\Phi_{LM}(t)$ represents the probability that a LM event (dilution of probe) takes place in one of the states A, I_1, I_2, FP by a time *t*. Because lipid mixing (and content mixing) involves diffusion, once it takes place, the signal persists even if the intermediate state evolves to a new state. In addition, the proposed mechanism is sequential and photobleaching is insignificant during our experiment, so the fractional fluorescence change can be expressed in the following form:

$$\Phi_{LM}(t) = \beta_0 A(t) + (\beta_0 + \beta_1) I_1(t) + (\beta_0 + \beta_1 + \beta_2) I_2(t) + (\beta_0 + \beta_1 + \beta_2 + \beta_3) FP(t), \quad (5)$$

where β_i is the probability that a fluorescence event leading to the observed signal happens in state *i* (A, I_1, I_2, or FP). We define the probabilities, β_i, to be normalized, so that the probability of observing a fusion property during all fusion intermediate states is always one. Thus, $\beta_1 + \beta_2 + \beta_3 = 1$, meaning that all lipid mixing had to have occurred in states I_1, I_2, or FP. Equation 3 yields:

$$\frac{dA(0)}{dt} = -k_1, \frac{dI_1(0)}{dt} = k_1, \frac{dI_2(0)}{dt} = 0, \frac{dFP(0)}{dt} = 0.$$

Because lipid mixing always began without delay, this means that mixing of lipids between fusing vesicles started in a state whose time derivative is nonzero and positive. The first state where these conditions hold is I_1, and therefore $\beta_0 = 0$. In addition, each observable must ultimately reach its final value when the system reaches its final state: $FP = 1$ and $A = I_1 = I_2 = 0$.

Description of the time course of LM always required two and only two exponential functions. For systems that could be described in terms of a one-intermediate model, this is understandable (see Appendix I). For systems requiring a two-intermediate model, there are two possible explanations for this: either the term containing a third exponential, which is present in the system's state evolution (Eq. 3), is negligible and can be omitted; or two of the three rate constants are very close and indistinguishable. However, nearly all systems we examined required two intermediates, and it is very unlikely that two of the three rate constants implied by this model are equal in every system. Therefore, we needed to consider which fusion state S_i would not contribute significantly to LM. Two out of four states ($I_2(t)$ and $FP(t)$) depend on all three exponents, according to Eq. 3. If we exclude those states from Eq. 5, we would have to conclude that lipid mixing takes place only in the I_1 state, which would be physically unreasonable. Another, more physically reasonable possibility is that lipid mixing is nearly completed in the second intermediate state I_2, i.e., $\beta_3 \approx 0$ and $\beta_1 + \beta_2 + \beta_3 \approx \beta_1 + \beta_2 \approx 1$. This does not mean that no lipid mixing occurs in FP, just that lipid mixing in this state is very small. This allows us to simplify Eq. 5 to obtain:

$$\Phi_{LM}(t) = \beta_1 I_1(t) + (\beta_1 + \beta_2) I_2(t) + FP(t), \quad (6)$$

which, due to normalization of the state functions S_i ($I_2(t) + FP(t) = 1 - (A(t) + I_1(t))$), gives

$$\Phi_{LM}(t) = 1 - A(t) + (\beta_1 - 1) I_1(t). \quad (6a)$$

Because terms containing I_2 and FP are eliminated, the time course of lipid mixing becomes double exponential (with rates k_1 and k_2 or k_1 and k_3; see Eq. 3). Note that assuming that $\beta_2 \approx 0$, also a plausible assumption, does not allow for this rearrangement and therefore does not remove the third exponential. In addition, mixing of lipids between the two *trans*-leaflets may be significant in I_2, as will be considered in the Discussion. Thus, setting β_3 approximately equal to zero seems appropriate and is necessary to account for the observation of only two exponentials. This could be seen as surprising, because pore formation occurs in FP and involves inner leaflet mixing. However, total lipid mixing is always much greater than total contents mixing, and the small amount of mixing between *trans*-leaflets that remains

T_R in the last step is likely too small a part of the total to be detected.

Leakage and content mixing

Content mixing (CM) is observed in our assays through binding of Tb^{3+} to DPA, and, if the vesicles are nonleaky, the content mixing fractional fluorescence change can be expressed in a way analogous to Eq. 5:

$$\Phi_{CM}^{\text{non-leaky}}(t) = \alpha_0 A(t) + (\alpha_0 + \alpha_1) I_1(t) + (\alpha_0 + \alpha_1 + \alpha_2) I_2(t) + (\alpha_0 + \alpha_1 + \alpha_2 + \alpha_3) FP(t). \quad (7)$$

Like the probabilities of lipid mixing, the probabilities of content mixing accumulate since content diffusion between trapped compartments is an irreversible event. The probability that a content-mixing event (leading to a fluorescence change) occurs in each state, α_i, (compare to β_i in Eqs. 5 and 6) is related to the permeability of the contact between vesicles, to the concentrations of Tb^{3+} and DPA in the contacting vesicles, and to the equilibrium constant of binding of Tb^{3+} to DPA. Permeability will be very low in the absence of a pore and, when a pore forms, will be limited by pore properties (size, opening time, molecular nature, etc.) and diffusion. A pore in state FP is by definition large and stable, whereas a pore in I_1 or I_2 could be transient and small (8,34). Even so, α_1 and α_2 could become significant if the probability of pore formation in I_1 or I_2 becomes significant. The standard state taken to define complete content mixing is vesicles containing coencapsulated Tb^{3+} and DPA, which is also the initial state for leakage (L) experiments and which has a fluorescence $F_L(0)$. Thus, the asymptotic fraction of ''possible'' content mixing is $f_{CM} = [F_{CM}(\infty) - F_{detergent}]/[F_L(0) - F_{detergent}]$. This same equation was used to describe inner leaflet mixing, which is expected only upon pore formation, and thus should track content mixing.

The content mixing signal is complicated by the fact that some of the vesicle contents escape during the fusion process and are no longer available for content mixing. Leakage is diffusion of trapped contents through the membrane bilayer into the external compartment. For reasons that will become apparent, we express leakage in terms of the fraction of trapped contents remaining after some time t. Thus, it can be expressed just as were the content-mixing and lipid-mixing signals in Eq. 6, except that the fraction of trapped probes available to leak ($(\Phi_L(t))$ starts at 1 and goes to 0 with time, whereas $\Phi_{LM}(t)$ and $\Phi_{CM}(t)$ both start at 0 and go to 1. The observables that define Φ_L are the fluorescence of vesicles with coencapsulated Tb^{3+} and DPA at time 0 ($F_L(0)$) as well as the fluorescence of these vesicles after addition of detergent to release their contents.

The rate of leakage, unlike the probabilities of content or lipid mixing, is a property associated with each state, i.e., not an accumulating property. The reversible properties considered (pyrene-cholesterol FRET ratio and light scattering) were also treated as nonaccumulating properties associated with individual states. Because the rate of leakage is proportional to the number of trapped probes, it is also proportional to $\Phi_L(t)$, and leakage can be described by the following differential equation:

$$\frac{d\Phi_L(t)}{dt} = -\Phi_L(t) \times (A(t)\lambda_0 + I_1(t)\lambda_1 + I_2(t)\lambda_2), \quad (8a)$$

where λ_i is the rate constant for leakage in state i. An important feature of all our data sets is that the time courses of content and lipid mixing are monotonic saturating functions, suggesting that the last state, FP, does not exhibit leakage or, at least, leakage from this state can be neglected within the observation time. Thus, we did not include a term for leakage in the final state, FP (i.e., $\lambda_3 = 0$).

Now that we have an expression for $\Phi_L(t)$, we are able to consider content mixing in a leaky system. The total change in fluorescence signal due to content mixing is caused by two fluxes: one that leads to an increase (superscript ''+''), and a second that leads to a decrease (superscript ''−'') in signal:

$$\frac{d\Phi_{CM}(t)}{dt} = J^+(t) + J^-(t).$$

The first term is caused by formation of fluorescent Tb^{3+}-DPA complex due to content mixing. The second term reflects a loss of fluorescent complex caused by leakage of complex out of vesicles. The first term is given by the derivative of Eq. 6 (for LM), except that we specify that the signal (F_{CM}) and probabilities (α_i) are for content mixing. The second term is given by Eq. 7, except that it specifies leakage only of Tb^{3+}-DPA complex and thus is proportional to $\Phi_{CM}(t)$ and not to $\Phi_L(t)$:

$$\frac{d\Phi_{CM}(t)}{dt} = \alpha_1 \frac{dI_1(t)}{dt} + (\alpha_1 + \alpha_2)\frac{dI_2(t)}{dt} + \frac{dFP(t)}{dt} - \Phi_{CM}(t) \times (A(t)\lambda_0 + I_1(t)\lambda_1 + I_2(t)\lambda_2), \quad (8b)$$

where we have used the observation that $\alpha_0 = 0$. The normalization condition ($\alpha_1 + \alpha_2 + \alpha_3 = 1$) further reduces the number of parameters.

THE SOLUTION

Analytical solutions can be obtained for two of the three observed quantities:

$$\Phi_{LM}(t) = \beta_1 \frac{k_1 - k_2}{k_1 - k_2}\left(1 - e^{-k_1 t}\right) + (1 - \beta_1)\frac{k_1}{k_1 - k_2}\left(1 - e^{-k_2 t}\right) \quad (9a)$$

$$\Phi_L(t) = e^{-\lambda_0 \frac{\left(1-e^{-k_1 t}\right)}{k_1}} e^{-\lambda_1 \frac{\left(1-e^{-k_1 t}\right)\times I_{11} k_2 + \left(1-e^{-k_2 t}\right)\times I_{12} k_1}{k_1 k_2}} \times e^{-\lambda_2 \frac{\left(1-e^{-k_1 t}\right) I_{21} k_2 k_3 + \left(1-e^{-k_2 t}\right) I_{22} k_1 k_3 + \left(1-e^{-k_3 t}\right) I_{23} k_1 k_2}{k_1 k_2 k_3}}, \quad (9b)$$

where

$$I_{11} = -\frac{k_1}{(k_1 - k_2)}, \quad I_{12} = \frac{k_1}{(k_1 - k_2)};$$
$$I_{21} = -\frac{k_1 k_2}{(k_1 - k_2)(k_3 - k_1)}, \quad I_{22} = -\frac{k_1 k_2}{(k_1 - k_2)(k_2 - k_3)},$$
$$I_{23} = -\frac{k_1 k_2}{(k_2 - k_3)(k_3 - k_1)}.$$

Reference to Eq. 8 makes it clear that a closed form solution for the time evolution of content mixing cannot be obtained analytically. Although a numerical solution would have been possible, it was desirable to obtain a solution that was suitable for use with a simple nonlinear regression routine, such as contained in the SigmaPlot package (v. 6.0, SPSS, Chicago, IL). For this reason, we used a simplification algorithm described in Appendix II.

Model evaluation through comparison to experiment

The sequential, two-intermediate model has 15 parameters: three rate constants and 12 parameters that describe the probabilities of lipid mixing, content mixing, and leakage in each state. Although four of these probabilities can be set to zero by observation $\{\alpha_0 = 0, \beta_0 = 0, \beta_3 = 0, \lambda_3 = 0\}$ and two normalization conditions constrain another two, this still leaves nine parameters (three rate constants, two λ_i and four α_i, and β_i probabilities) whose values must be determined by comparison to experiment. The process of fitting three data sets simultaneously while adjusting nine model parameters is a daunting computational task. Thus, we broke the task down into a series of steps in which a limited number of parameters were determined from each of the data sets using SigmaPlot (v. 6.0, SPSS) to perform regression analysis, and then an additional step in which these parameters were tested for self-consistency. To avoid possible distortions in the time courses that might be caused by normalization, we fit raw fluorescence data in all cases. The procedure was as follows:

1. The lipid mixing time course was fit to obtain the rates k_1 and k_2 as well as the lipid mixing probabilities β_1 ($\beta_2 = 1 - \beta_1$) using Eqs. 3, 4, and 6.
2. The leakage and content mixing time courses were globally fit to obtain the leakage coefficients, λ_0 and λ_1, the rate k_3 and the CM probabilities α_1 and α_2 using Eqs. 3, 4, and 8a,b. In one instance (DOPC/DOPE/CH 22 nm vesicles, Fig. 2), it was not possible to determine k_3 from contents-mixing and leakage data, and it was determined using other observations (see Results).
3. Because our fitting used an analytical approximation described in Appendix II, we checked the solutions by directly solving Eq. 8b using the Runge-Kutta method (35). If the values obtained from fitting are correct, the numerical solution with the parameters obtained from fitting should correspond well with experimental data.
4. Next, we tested the ability of the model, with the rate constants k_1, k_2, and k_3 fixed as described above, to account for the time courses of light scattering and PY-CH excimer/monomer intensity ratio during PEG-mediated fusion, with the intensity values for these phenomena being adjusted not as probabilities but as the values of light scattering intensity and PY-CH E/M ratio associated with each state. In most cases, this procedure produced a self-consistent explanation of all five time courses. When deviations from this simple algorithm were necessary, these are described in Results.

To test the parameters from global fits, we also used an iterative algorithm in which the leakage time course was first fit to obtain the leakage coefficients, λ_0 and λ_1, and the rate k_3 using Eqs. 3, 4, and 8a. Then the content mixing time course was fitted to obtain the CM probabilities α_1 and α_2 using the same equations. These values were then fixed and k_3 was varied to optimize the fit. This value was used to adjust λ_0 and λ_1 while fitting leakage data. This procedure was repeated until parameter values converged. All parameter values reported here were obtained using the global fitting procedure unless otherwise indicated.

Although regression analysis was a multistep process, and thus could not yield a global statistical analysis, *P*-values for most individual parameters at each step of the process were always <0.0001. To judge the uniqueness of a fit, we began regression analysis with different initial parameter values and, for reasonable initial parameter estimates, we always came to the same ''best-fit'' parameters for each data set. Obviously, this does not guarantee that parameter values are unique, but multiple searches from different regions of parameter space are often the best that one can do to test for a unique fit. Finally, for all cases save one (DOPC/DOPE/CH 110 nm vesicles), the parameter values obtained by global analysis were essentially the same as obtained by the alternative iterative algorithm.

RESULTS

Lipid mixing, content mixing, and leakage time courses from five vesicle systems

Fig. 2 presents the results of fitting time courses associated with 5% PEG-induced fusion of 22 nm vesicles composed of DOPC/DOPE/CH (50:25:25). The experimental data are taken from Malinin and Lentz (17). In addition to the three basic data sets (*panel A*, lipid mixing; *panel B*, leakage; and *panel C*, content mixing), inner leaflet mixing (*panel A*, *solid circles*) light scattering (*panel E*), and PY-CH E/M ratio (*panel D*) were also followed. The lipid mixing data were fit as described in ''Data analysis'' to obtain the rate constants k_1 and k_2. For this system, the content mixing and content leakage data were insufficient to fix k_3. We attempted to determine k_3 using measurements of lipid mixing between noncontacting inner leaflets of PEG-aggregated vesicles

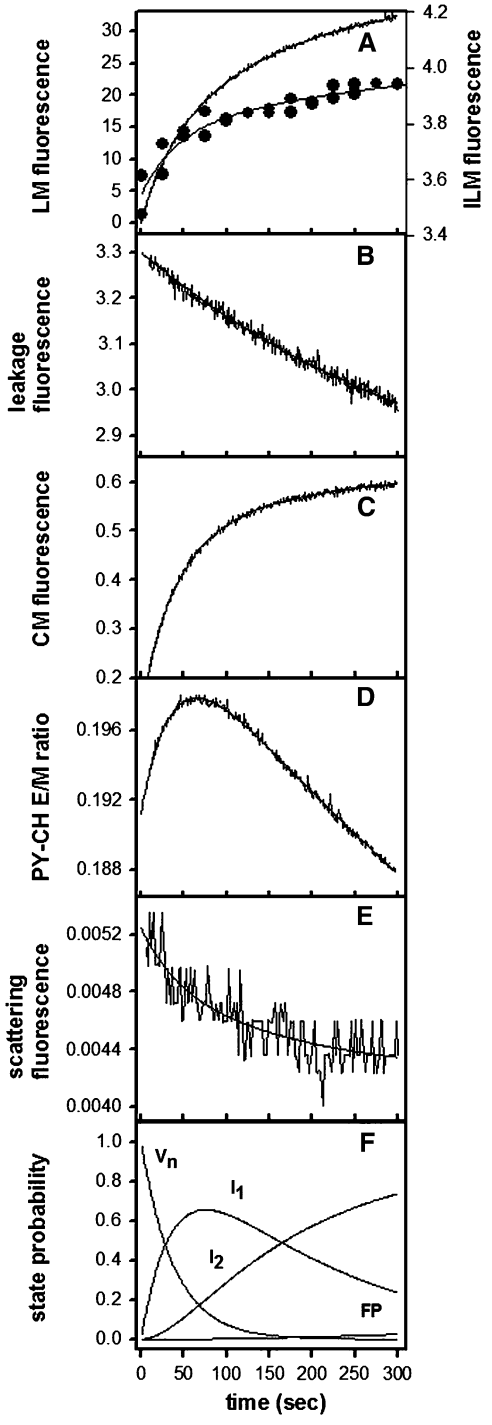

FIGURE 2 Time courses are shown for five observables (*A*, lipid mixing; *B*, leakage; *C*, content mixing; *D*, PY-CH excimer/monomer fluorescence ratio; and *E*, 90° light scattering) characterizing fusion of DOPC/DOPE/CH (50:25:25) 22 nm vesicles induced by 5 wt% PEG. Solid circles in panel *A* report inner leaflet mixing, as plotted on the right *y* axis. The solid lines show the fit of the sequential model to these data, with parameters summarized in Table 1. The evolution of proposed states with time during the fusion process is shown in panel *F*. The buffer was 800 mM NaCI, 10 mM TES, and 1 mM EDTA, chosen so as to balance the molality of the trapped and exterior volumes after addition of the vesicles to 5 wt% PEG.

(Fig. 2 *A*). However, inner leaflet lipid mixing did not saturate sufficiently at long time to define k_3. Thus, k_3 was determined for this system using the time dependence of cholesteryl-pyruvate excimer/monomer fluorescence ratio. We have shown previously that this ratio increases with the formation of fusion intermediates and then decreases at a rate that characterizes fusion pore formation (17). The content mixing and leakage data were then used to determine the α and λ values. The rate constants k_1, k_2, and k_3 thus determined were able to describe both inner leaflet mixing and light scattering data. The results of this process are shown by smooth curves through the data in Fig. 2, with the best-fit parameters given in data row 1 of Table 1. Finally, the predicted evolution of the fusion states S_i is presented in panel *F*, as obtained using k_1, k_2, and k_3 and the expressions in Eq. 3. We note that none of the five experimental time courses show a delay that is characteristic of sequential processes, despite the prediction that the appearance of I_2 and FP are delayed. The absence of an observable delay, particularly in content mixing, means that some movement of contents between vesicle compartments must occur in the intermediates I_1 and I_2 (see α_1 and α_2 in Table 1). The fact that leakage in these systems also showed no delay implies that the A state shows substantial content leakage for this vesicle composition (see λ_0, data row 1 in Table 1), which is rich in DOPE, a bilayer destabilizing lipid.

A three-intermediate model provided a slightly improved description of the data (slightly lower reduced χ^2), but the increased number of parameters made all parameters poorly defined. The two-intermediate, parallel stalk model was also tried, but, for reasons laid out in ''Models considered'', this model could not describe all the data. Models with more than four states were not considered, as these required more unknown parameters and thus cannot be considered simpler than the two-intermediate model. The two-intermediate model was the simplest model that can provide a general description of PEG-mediated fusion of DOPC/DOPE/CH (50:25:25) 22 nm) vesicles.

For all other systems considered, the lipid mixing, content mixing, and content leakage data were sufficient to determine the three rate constants. Fig. 3 presents fusion time courses obtained at 5 wt % PEG for DOPC/DOPE/SM/CH (35:30:15:20) 25 nm vesicles prepared in 800 mM NaCl, 10 mM TES (pH 7.4) buffer. The high salt buffer was used so that the interior and exterior compartments of the vesicles were osmotically balanced (11). This avoids the compressive osmotic force that occurs when vesicles containing 100 mM NaCl are induced to fuse using externally added PEG. Again, the time courses of all five observables were well described by the two-intermediate sequential kinetic model (data row 2 in Table 1). In contrast to DOPC/DOPE/CH (50:25:25) 22 nm vesicles (Fig. 2), these vesicles show a lag in content leakage (*panel B*), suggesting that leakage is delayed until state I_1 or I_2. A good fit was obtained by assigning all leakage to state I_2 ($\lambda_0 = \lambda_1 = 0$ in data row 2 in Table 1).

TABLE 1 Parameters defined by nonlinear regression of fusion time courses for the systems mentioned in the text

System	$k_1 \times 10^3$ (s^{-1})	$k_2 \times 10^3$ (s^{-1})	$k_3 \times 10^3$ (s^{-1})	Content mixing				Lipid mixing				Leakage rates $\times 10^4$ (s^{-1})			Reference from which data taken
				α_1 (I_1)	α_2 (I_2)	α_3 (FP)	f_{CM}	β_1 (I_1)	β_2 (I_2)	β_3 (FP)	f_{LM}	λ_0 (I_0)	λ_1 (I_1)	λ_2 (I_2)	
DOPC-DOPE-CH, 22 nm vesicles, 5 wt% PEG	26 ± 2	5.6 ± 0.4	0.20 ± 0.07*	0.33 ± 0.01	0.46 ± 0.02	0.21 ± 0.02	0.23	0.48 ± 0.09	0.52 ± 0.09	0	0.32	5.8 ± 0.2	4.2 ± 0.2	2.6 ± 0.2	(17)
DOPC-DOPE-SM-CH, 25 nm vesicles, 800 mM NaCl, 5 wt% PEG	24.4 ± 0.8	3.05 ± 0.09	1.0 ± 0.2	0.227 ± 0.003	0.773 ± 0.005	0	0.06	0.274 ± 0.005	0.726 ± 0.005	0	0.26	0	0	1.75 ± 0.04	(11)
DOPC-DOPE-SM-CH, 25 nm vesicles, 100 mM NaCl, 5 wt% PEG	22 ± 0.7	S	3.75 ± 0.03	0.202 ± 0.006	S	0.798 ± 0.006	0.051	0.27 ± 0.03	S	0.73 ± 0.03	0.410	0	1.54 ± 0.02	S	This article
DOPC-DOPE-SM-CH-PS, 20 nm vesicles, 6 wt% PEG	7 ± 3	1.4 ± 0.4	10 ± 2	0.38 ± 0.02	0.5 ± 0.2	0.12 ± 0.2	0.06	0.26 ± 0.07	0.74 ± 0.07	0	0.18	0	0	4.3 ± 0.7	(33)
DOPC-DLPC, 20 nm vesicles, 17.5 wt% PEG	57 ± 1	7.4 ± 0.1	3.3 ± 0.2	0.06 ± 0.01	0.44 ± 0.02	0.50 ± 0.02	0.05	0.69 ± 0.02	0.3116 ± 0.02	0	0.33	0	0.4 ± 0.1	1.35 ± 0.09	(12)
DOPC-DOPE-CH, 110 nm vesicles, 5 wt% PEG	2.12 ± 0.01	S	0.33‡	0.55 ± 0.03	S	0.45 ± 0.03	0.02	1.00 ± 0.02	S	0.00 ± 0.02	0.11	1.86 ± 0.01	0	S	This article
DOPC/$DC_{18:3}$PC, 45 nm vesicles, 17.5 wt% PEG†	80	6	8	0	0	1	S	0.71	0	0.29	S	0	0	0	(8)

$\alpha_0(A) = 0$, $\beta_0(A) = 0$, $\beta_3(FP) = 0$, $\lambda_3(FP) = 0$.
*The rate was found from the PY-CH excimer/monomer fluorescence ratio data, Fig. 2.
†This set was fitted manually.
‡The value was found from the straight line shown in Fig. 8, i.e., through equation: $k_2 = 0.1539\ k_1$; k_1 was found through single exponential fit.
S, assumed that only I_1 and FP exist for two intermediate system.

We observed for DOPC/DOPE/SM/CH/DOPS (32:25:15:20:8) 20 nm vesicles (36), which fused in the presence of 6 wt% PEG, a similar delay in leakage (data not shown but parameters summarized in data row 4 of Table 1) as seen with the osmotically balanced DOPC/DOPE/SM/CH (35:30:15:20) 25 nm vesicles. The presence of SM in these vesicles has previously been noted to make them stable and resistant to leakage (10). As noted above, the parallel stalk model (Scheme 2b) could not account for the behavior of this or other systems having no leakage associated with the initial intermediate.

We also examined osmotically unbalanced DOPC/DOPE/SM/CH (35:30:15:20) 25 nm vesicles (made with 100 mM NaCl buffer) at 5 wt% PEG, as summarized in data row 3 of Table 1. These data were adequately described by a single exponential function, meaning that there is effectively only a single intermediate state that proceeds directly to a fusion pore (FP state). We have no way to determine whether this intermediate might be I_1 or I_2, but this is immaterial, because the observation of only a single intermediate shows that the free energy barrier between the two is so small that these two states are indistinguishable. We have arbitrarily assigned the single intermediate state for this system as I_1 (data row 3 in Table 1, where we have noted this assumption with ''S''); thus, k_3 is here the rate of conversion of I_1 to FP. In instances when only a single intermediate and FP state are presumed to exist, we still observe two components of lipid mixing, meaning that observable lipid mixing must occur in the FP state under these conditions. For all systems with single-exponential content mixing examined thus far, this is a consistent result for, since lipid mixing was always double exponential. Note that $\lambda_0 = 0$ in the osmotically unbalanced vesicles just as in the osmotically balanced vesicles, meaning again that leakage was delayed until I_1 or I_2. Because only one intermediate was observed in this case, leakage was assigned to I_1. Comparison of the results in rows 2 and 3 shows that the effect of a compressive osmotic gradient was to lower or eliminate the barrier between the I_1 and I_2 states, making the I_2 state irrelevant. This possibility was suggested previously based on calculations of the free energy profile of the fusion process (18).

The proposed two-intermediate model was also successful in describing the kinetics of three other vesicle systems (data

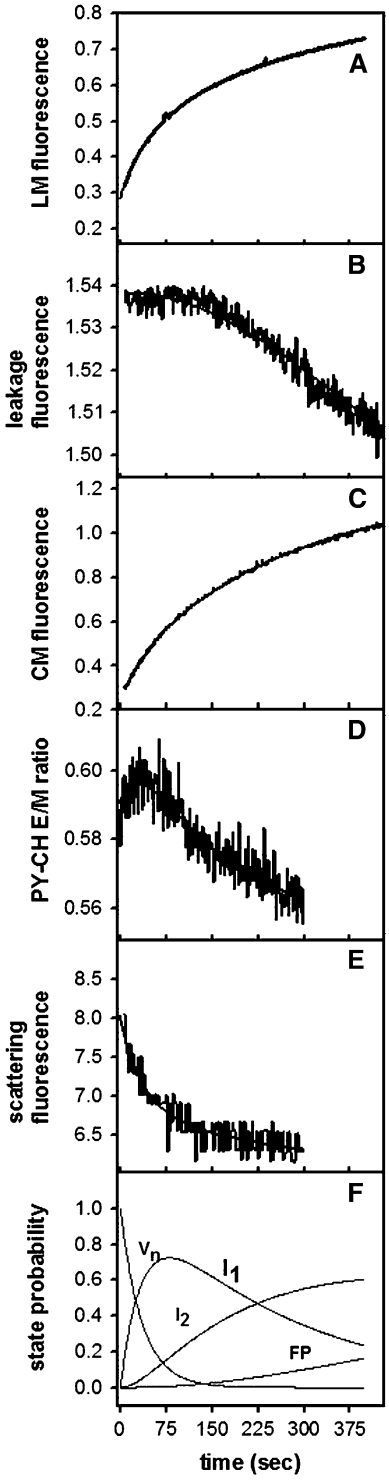

FIGURE 3 Time courses are shown for five observables (*A*, lipid mixing; *B*, leakage; *C*, content mixing; *D*, PY-CH excimer/monomer fluorescence ratio; and *E*, 90° light scattering) characterizing fusion of POPC/POPE/SM/CH (35:30:15:20) 25 nm vesicles at 5 wt% PEG. The solid lines show the fit of the sequential model to these data, with parameters summarized in Table 1. The lag in leakage at early times suggests minimal leakage in one or two of the proposed intermediates (I_1 and I_2). The evolution of states with time during the fusion process is shown in panel *F*. The buffer was 800 mM NaCl, 10 mM TES, and 1 mM EDTA.

not shown). Fusion of fusion-resistant DOPC/DLPC (85:15) 20 nm vesicles was observed at 17.5 wt% PEG (12), and these data also required a two-intermediate model (data row 5 in Table 1). In the sixth system analyzed, DOPC/DOPE/CH (50:25:25) 110 nm vesicles at 5 wt% PEG, a single-intermediate model again provided an adequate description of the data (data row 6 in Table 1). In this system, the leakage rate is substantial, and the very small amount (2%) of content mixing observed is completed in two states, again meaning that I_1 and I_2 are indistinguishable for this system. Just as for osmotically unbalanced DOPC/DOPE/SM/CH 25 nm vesicles (row 3 of Table 1), we assigned the intermediate state as I_1 (i.e., $\beta_2 \approx 0$). Because content mixing was so limited in this system, it was difficult to assign the probabilities α_1 and α_2. Thus, the values obtained by the iterative fitting method (0.13 and 0.87, respectively) differed somewhat from those obtained by the global fitting method (0.31 and 0.69) given in Table 1. It is significant that, even for the only system in which the two fitting methods produced somewhat different parameter values, the basic behavior of the system was the same for both fitting procedures.

From the six systems described so far, it is clear that there is a finite probability of content mixing in the intermediate states, not just in the final pore (FP) state. In all of these systems, leakage of contents also occurred in one or more intermediate states. A special case of a nonleaky system was described in Lee and Lentz (8), where complete separation of outer and inner leaflet lipid mixing was observed during 17.5 wt% PEG-induced fusion of DOPC/1,2-dilinolenoyl-*sn*-phosphatidylcholine ($DC_{18:3}PC$) (85:15) 45 nm vesicles. No leakage of Tb^{3+}/DPA was observed in this system, and mixing of Tb^{3+} and DPA contents occurred along with inner leaflet mixing, confirming fusion pore formation. However, some leakage of protons across bilayers was observed throughout fusion, and proton movement between vesicle compartments was also observed during both I_1 and FP formation (8). The clear separation between I_1 and FP states and the ability to isolate an irreversible state after I_1 and before FP were seen as experimental support for the two-intermediate model. Fig. 4 shows that the current analysis can also describe the inner leaflet mixing (*open squares*), total lipid mixing (*open circles*), and content mixing (*solid circles*) for DOPC/$DC_{18:3}PC$ 45 nm vesicles. The parameter values that provide these fits are given in data row 7 of Table 1. The β-values for inner leaflet mixing were taken as the α-values for content mixing, since content and inner leaflet lipid mixing are associated with the same event, pore formation; β-values in Table 1 are probabilities of total lipid mixing. This analysis indicates that inner leaflet mixing and content mixing in this system took place only in the final, FP, state (Table 1). Outer leaflet mixing occurred primarily in the first intermediate, I_1. The analysis required a second intermediate (I_2) to account for the separation of inner and outer leaflet mixing, but this intermediate was inactive in that no content or lipid mixing (inner or outer leaflet) took place in

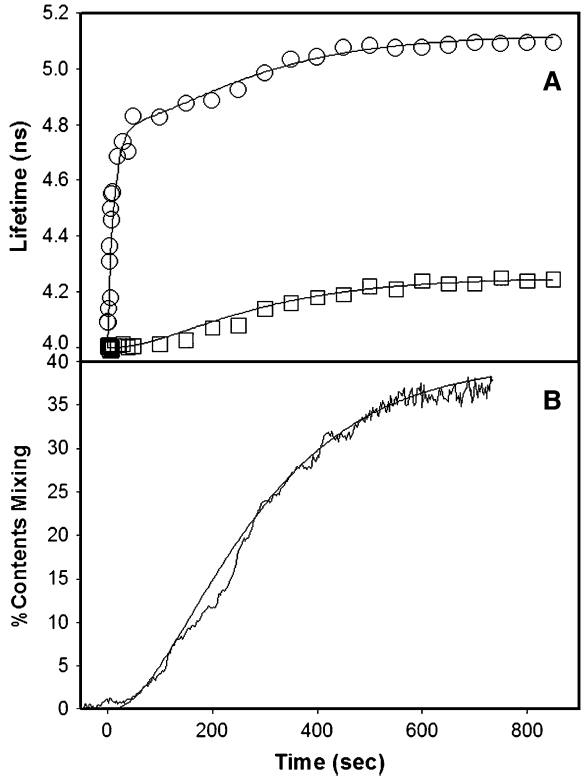

FIGURE 4 The inner leaflet (*squares*) and total (*circles*) lipid mixing time courses for DOPC/$DC_{18:3}$PC (85:15) 45 nm vesicles induced by 17.5 wt% PEG (8) are shown in panel *A* as the lifetime (*left axis*) of the fluorescent probe DPHpPC. The time course of fluorescence change due to mixing of Tb^{3+} with DPA is shown in panel *B*. The fits to these data obtained with the sequential model with two-intermediate states are also shown as solid lines, with the parameters yielding these fits presented in row 7 of Table 1. The unique features of these data derived from the completion of outer lipid mixing completed in state I_1, with no lipid mixing in state I_2, and inner leaflet lipid mixing and content mixing taking place only in the FP state.

this state ($\beta_2 = \alpha_1 = \alpha_2 = 0$ in Table 1). This system is clearly unique in that it required three exponentials to describe fusion kinetics, whereas all others required only two. However, two other systems also showed no lipid mixing in the I_2 state but then lipid mixing in the FP state (rows 3 and 6 of Table 1), in contradiction to our assumption that lipid mixing should be negligible in the FP state. However, the I_2 state was not detected in these two systems (i.e., no fusion observables were associated with it). This permitted description of content mixing and lipid mixing kinetics in terms of only two exponentials without the assumption that $\beta_3 = 0$. In DOPC/$DC_{18:3}$PC 45 nm vesicles, however, the I_2 state was essential to describe the time course of fusion, but did not contribute to any fusion observables. We suggest from these analyses that, if lipid mixing is negligible in I_2, it can be detectable in FP. This is physically reasonable and does not violate the spirit of our assumption that $\beta_3 \approx 0$ when significant lipid mixing occurs in I_1 and I_2. Note that our analysis indicates that this system follows the classical stalk model (2), in which content mixing occurs only after a hemifused intermediate (I_1) even though the inactive I_2 state was essential to accommodate these data.

Testing model parameters using additional observables

Assumption of irreversibility

As described under ''Data analysis'', the nine free parameters of the model were fixed based on fitting three basic data sets (lipid and content mixing, leakage, Figs. 2 and 3, *A–C*). In most cases, these data sets were sufficient to define the model parameters. However, we checked the model and the validity of rate constants by using these to describe two additional experiments: right angle light scattering, as a measure of lipid structural rearrangements, and the Py-CH E/M ratio (Figs. 2 and 3, *D* and *E*) that reports the presence of nonlamellar intermediates during the fusion process (17). Light scattering from 20 to 26 nm vesicles was not intense but jumped very rapidly (<1 s, not shown) as vesicles aggregated in the presence of PEG. This was expected, because PEG-induced aggregation is much faster than subsequent fusion events (8,12). After rapid aggregation, light scattering declined, implying changes in structure of the different states of the fusion process that progressively reduce the local gradient of refractive index, as one might expect as juxtaposed bilayers merge. The same model and its associated rate constants (k_1, k_2, k_3 in Table 1) accounted for these two sets of data with the adjustment only of the probabilities that these properties were associated with different states. It should be stressed that the three basic observables (lipid mixing, content mixing, and leakage) were sufficient to determine all the rate constants, and that the additional observations were used just to test these rate constants and the model. This observation has two important implications. First, it supports the two-intermediate model, as the time dependence of five observables was described by the three rate constants derived from this model. Second, these additional observables report lipid microstructures in the intermediate states. Unlike lipid mixing, content mixing, and leakage, formation of these microstructures should be reversible. Nonetheless, the time dependence of these observables is explained by the three kinetic constants derived from fitting irreversible observables to an irreversible model. This argues strongly for the validity of our assumption that the rates of the reverse reactions for step 1 and possibly step 2 of the two-intermediate, sequential model are insignificant.

Kinetic behavior as a function of PEG concentration

Although comparison of these seven vesicle systems was useful for testing the validity of the sequential model, comparing data from many lipid systems limits our ability to look for relationships between events in the fusion process. To look for systematic relationships between the model

parameters and thereby gain more insight into the fusion process, we examined a single simple vesicle system as a function of PEG concentration. We used DOPC/DOPE/SM/CH (35:30:15:20) 25 nm vesicles at PEG concentrations of 0, 1, 2, 4, 5, 7, and 10 wt%. Time courses of lipid mixing, content mixing, and leakage (Fig. 5) were adequately described by the single-intermediate model at all PEG concentrations (*smooth curves* in Fig.5). In single-intermediate systems, we envision I_1 and I_2 to be indistinguishable and the resolved rate constants to be k_1 and k_3, where k_3 here represents the rate of formation of a pore directly from the I_1 state. In these experiments, membranes were driven into increasingly closer contact by increasing concentrations of PEG, leading to increasing fractions of productive contacts

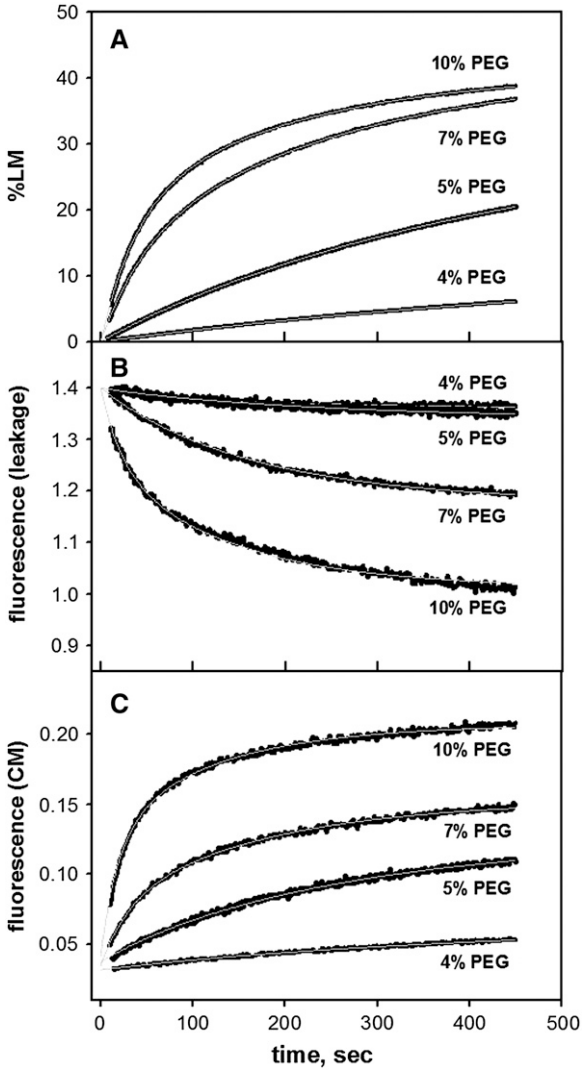

FIGURE 5 Time courses are shown for three observables (*A*, lipid mixing; *B*, leakage; *C*, content mixing) characterizing fusion of DOPC/DOPE/SM/CH (35:30:15:20) 25 nm vesicles induced by different concentrations of PEG. The solid black lines through the data represent the fit of a single-intermediate, sequential model to the data. The buffer was 100 mM NaCI, 10 mM TES, and 1 mM EDTA.

(f_{LM} shown as *diamonds* in Fig. 6), with the first such contacts recorded at 4 wt% PEG. A low rate of lipid mixing was observed for PEG concentrations <4 wt%, but this rate was too slow to establish an end point and to define f_{LM}, which is plotted in Fig. 6 (*diamonds*) at and above 4 wt% PEG. Small rates of content mixing were also detected at 4 wt% PEG (Fig. 5, *B* and *C*), with f_{CM} plotted as circles in Fig. 6. Thus, 4 wt% PEG was found to be the threshold for observing productive intervesicle contacts leading to fusion. The probabilities of fusion events (CM, *solid squares*; LM, *solid triangles*) taking place in the intermediate state also increased with PEG concentration (Fig. 7 *A*), as did the rate of content leakage (Fig. 7 *B*). These results show that content mixing took place mainly in the FP state at low PEG, but occurred increasingly in the I_1 state as PEG concentration increased. The rates of leakage in the A and I_1 states also increased as PEG concentration increased.

Both k_1 and k_3 seemed to increase with PEG concentration in this system once fusion began, as shown by the solid circles in Fig. 8, with k_1 being the abscissa and k_3 the ordinate. To test for this behavior in other systems, we plotted k_3 versus k_1 for two-intermediate systems as well, as shown by the diamonds in Fig. 8. There was clearly no correlation. However, the solid triangles shown in Fig. 8 demonstrate that k_2 is proportional to k_1 in two-intermediate systems, with roughly the same line of proportionality as for k_1 versus k_3 in single-intermediate systems. These correlations imply that a pore forms by a different mechanism in I_1 and I_2 (or in single-intermediate systems) than for FP. This suggests two types of content-mixing events, one that occurs early in the fusion process and one involved in making the final FP state.

A clue to the difference between these two events may be in the observation that FP is normally not observed to have the property of leakage. For two-intermediate systems, either state I_1 or I_2, or both, have the property of leakage in addition to lipid mixing and content mixing (Table 1). In single intermediate systems, I_1 displays leakage in one of the two

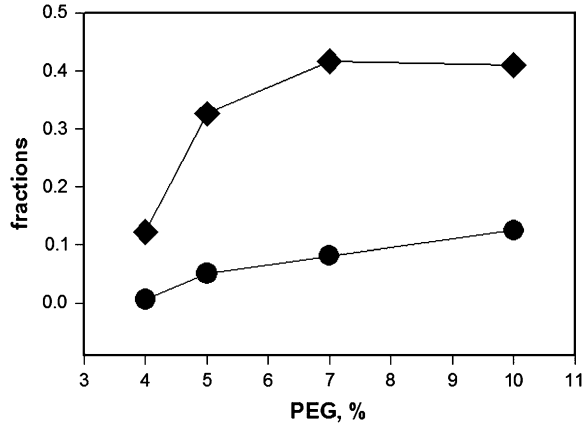

FIGURE 6 Fractions of maximal possible lipid mixing (f_{LM}, *diamonds*) and content mixing (f_{CM}, *circles*) are shown versus PEG concentration for fusion of DOPC/DOPE/SM/CH (35:30:15:20) 25 nm vesicles (see Fig. 5).

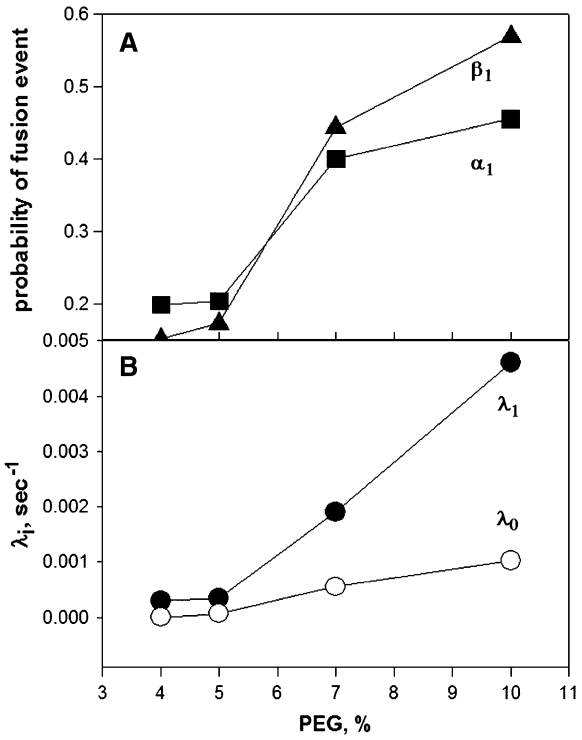

FIGURE 7 (*A*) Dependence of the lipid mixing (*triangles*, β_1) and content mixing (*squares*, α_1) probabilities in the intermediate state I_1 on PEG concentration for DOPC/DOPE/SM/CH (35:30:15:20) 25 nm vesicles, as derived from fitting the data in Fig. 5. Note that only one intermediate state is required to describe this system, so that the only other state in which lipid and content mixing occurs is FP. (*B*) Leakage rates of the A-state (λ_0, *solid circles*) and I_1-state (λ_1, *open circles*) as functions of PEG concentration for the same vesicle system.

systems examined. For both single intermediate systems, both I_1 and FP display content mixing and lipid mixing. To obtain a more quantitative view of the relationship between content mixing and leakage, we focused on the behavior of the single-intermediate system DOPC/DOPE/SM/CH (35:30:15:20) 25 nm vesicles at varying PEG concentrations. Fig. 9 shows that the probability of content mixing in I_1 (α_1) increased as the rate of leakage in either the A (*open triangles*) or I_1 (*solid triangles*) state increased. Necessarily, the probability of content mixing in the FP state ($\alpha_3 = 1 - \alpha_1$) decreased with leakage (*squares*). Note that content mixing occurs exclusively in state FP ($\alpha_1 = 0$ and $\alpha_3 = 1$) in the absence of leakage. This suggests that one of the two types of content-mixing events occurs early in the fusion process and is associated with leakage, whereas the other leads to the final nonleaky FP state. An interpretation of this in terms of the modified stalk hypothesis is given in the Discussion.

DISCUSSION

In this article, we aimed to answer four questions about PEG-mediated fusion formulated in the Introduction:

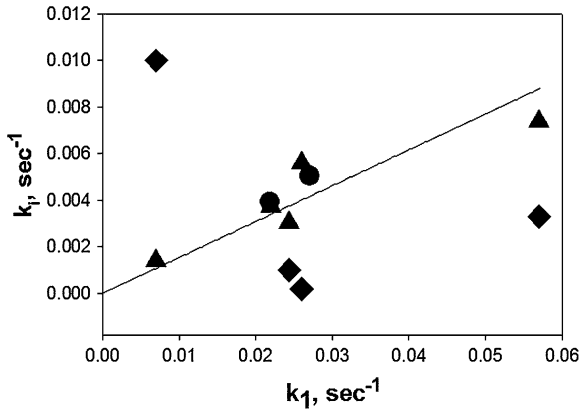

FIGURE 8 The rate constant k_3 is plotted versus k_1 for fusion via a single intermediate of DOPC/DOPE/SM/CH (35:30:15:20) 25 nm vesicles at 7 and 10 wt% PEG (*solid circles*). The triangles show k_2 versus k_1 for five two-intermediate systems presented in Table 1. The solid diamonds depict k_3 versus k_1 for these same two-intermediate systems (one diamond falls off the plot).

1. Can a sequential model explain the time course of the fusion process as reported by various measured events during PEG-mediated fusion? If so, what is the minimum number of intermediate states required to describe the observations?

A single-intermediate model was sufficient to model fusion of DOPC/DOPE/SM/CH (35:30:15:20) 25 nm vesicles and of DOPC/DOPE/CH 110 nm vesicles. However, we had to use the sequential, two-intermediate model to describe the five other systems considered. More complex models did not yield significantly better descriptions. Thus, the simplest model to describe all our kinetic data is a sequential, two-intermediate model.

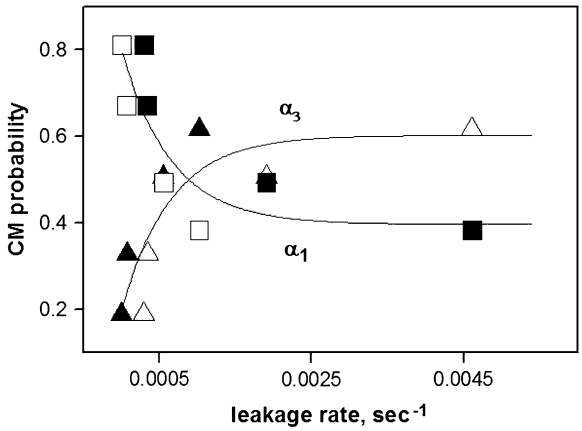

FIGURE 9 Correlation between content mixing probabilities, α_1 (*triangles*, I_1 state) and α_3 ($= 1 - \alpha_1$; *squares*, FP state), and leakage rates, λ_0 (*open symbols*, A state) and λ_1 (*solid symbols*, I_1 state), for DOPC/DOPE/SM/CH (35:30:15:20) 25 nm vesicles, as derived from fitting data in Fig. 5. Leakage in both states increased with PEG concentration.

2. What are the experimental observations necessary to define the kinetic and physical characteristics of the states identified in the simplest model?

Even though we used five data sets to verify our model (lipid and content mixing, leakage, right angle light scattering, and pyrene E/M ratio, Figs. 2 and 3), the minimum required data sets were content mixing, lipid mixing, and leakage.

3. Does the success of the sequential model offer support for the ''modified stalk'' hypothesis for the mechanism of lipidic pore formation during fusion?

The lipid-centric stalk model is not universally accepted, although there is considerable support for it (1,8,11,37). Two possible structures have been discussed with respect to this model for fusion: the stalk (2) and the TMC (5). We show here that a two-intermediate, sequential model can describe fusion in a variety of quite different vesicle systems as long as we recognize that intermediate states are ensembles of similar structures with average mechanical properties. Can we identify the two intermediates required by our analysis with these structures and thus offer support for the lipid-centric model? The properties of the I_1 state (LM, CM, and leakage) are consistent with the properties displayed by a Monte-Carlo-generated dynamic stalk (38). Based on calculations of the free energy profile of a hypothetical fusion reaction profile (6,7), we propose that I_2 consists of an ensemble of slightly expanded TMC-like structures, as described by Siegel (5). A slightly expanded TMC constitutes one of two of free energy minima revealed by these calculations. This proposal is also consistent with our observation that considerable mixing of lipids must occur in I_2, since evolution of a stalk to a TMC structure requires movement of lipid between *trans* and *cis* monolayers, a process that would seem more probable in the highly stressed lipid annulus that expands as the TMC forms and expands. We conclude that our results are consistent with a modified stalk model involving an ensemble of stalk-like states and a subsequent ensemble of TMC-like states. The structures proposed as intermediates by the modified stalk hypothesis are transient and cannot be directly demonstrated during fusion, but they are consistent with the two-intermediate, sequential kinetic model we propose here. Thus, analysis of kinetic experiments by the two-intermediate, sequential model provides a powerful means of testing the modified stalk hypothesis against experimental observation.

4. Does the model allow us to extract information related to functional properties of the fusion intermediate states?

In addition to the three kinetic constants that define the sequential evolution of fusion states, fitting our model to time courses of content and lipid mixing and content leakage yields the probabilities that these events occur in each state. These probabilities are functions of the lipid composition and curvature of the membranes, the force with which the membranes are pressed into contact, temperature, osmotic stress, the presence of membrane proteins, etc. Knowledge of the influence of each of these conditions on the properties of the different states of the fusion process can be used to test structural models, such as the ''stalk'' model of fusion.

If one accepts that our results support the ''modified-stalk'' model and assumes that kinetic intermediates we identify (I_1, and I_2) correspond to ensembles of the structural intermediates of the ''modified-stalk'' model (stalk and expanded TMC), we can also suggest an explanation for the results in Figs. 8 and 9 that support the existence of two types of content-mixing events. In nonleaky DOPC/$DC_{18:3}$PC (85:15) 45 nm vesicles, two types of content-mixing events were also observed: hydrogen ions moved between vesicles in I_1 (8) even though movement of larger solutes occurred only in FP, suggesting that early content mixing might be associated with flickering pores and later with stable fusion pores. If we identify state I_1 with an ensemble of stalk-like structures, then we can offer a possible mechanism for this observation. The stalk represents the initial free energy minimum on a presumed reaction path in which contacting or *trans*-monolayer join (6,7). This is a highly stressed structure in which significant fluctuation in monolayer structure is expected. As the stalk expands, a free energy barrier must be overcome to reach the second intermediate, the expanded TMC (6). In single-intermediate systems, this barrier is presumably so low that I_2 no longer exists as a distinct intermediate, and I_1 proceeds directly to FP. In a crude sense, the process of forming an initial stalk intermediate from juxtaposed highly curved bilayers is the reverse of forming a very small pore from a stalk intermediate. Because both the beginning and end sates of either process are highly stressed, it is expected that leakage might be a property of both the A and I_1 states in such systems. Thus, the rate of formation of I_1 from a leaky A state (k_1) correlates with the rate of FP formation from the leaky I_1 state (k_3) in a single-intermediate system (Fig. 8). In accord with the Monte Carlo simulations of Schick and colleagues (38), we suggest that fluctuations are responsible both for the leakage and for the signals of content mixing and inner leaflet lipid mixing that our analysis suggests are properties of the I_1 state.

In two-intermediate systems, I_1 must proceed to a final pore via I_2. The conversion of I_1 (ensemble of stalk-like structures) to I_2 (ensemble of extended TMC-like structures) is opposed primarily by the interstice free energy and then by a peak in the bending energy associated with the growth of the annulus around the expanding TMC structure (6). In the initial I_2 state, before the TMC expands, there should still be significant local stress and thus leakage and content mixing associated with leakage. As the annulus expands, significant curvature-related fluctuations away from the bilayer geometry are less concentrated since the very localized stress of the stalk is spread over a larger area. Ultimately, this may make fluctuation-related pores less likely. If such a situation occurs, fusion would need to proceed by a slower process not linked to leakage. This

would explain the existence of two types of pores leading to content mixing: leakage-related pores that occur early in the process (in I_1 and I_2) and then stable pores that occur late in the process when I_2 converts to FP. This would also account for the two types of pores revealed by electrophysiological measurements. Such measurements report ''flickering'' pores early in the fusion process (28,29,39), which are normally, but not always, followed by opening of a larger pore (3132). ''Flickering'' pores necessarily have a free energy close to but slightly larger than that of a closed state. This would be completely consistent with the fluctuation-related pores suggested by our results and the Monte Carlo simulations of Schick and colleagues (38).

Finally, our analysis supports the contention that PEG-mediated fusion occurs at a critical interbilayer spacing. We showed previously that an interbilayer distance of ~5 Å occurred at the threshold PEG concentrations needed to induce fusion in three two-component lipid mixtures (24). We suggest here that critical contacts are established once f_{LM} no longer increases with PEG concentration. Aggregation number determines the maximum extent of lipid mixing (f_{LM}), varies with vesicle size (8,12), and is likely not diffusion controlled. Thus, we expect the dependence of f_{LM} on PEG concentration to asymptote at the PEG concentration needed to establish optimal intermembrane contact. Fig. 6 shows that 5–7 wt% PEG is required to obtain optimal f_{LM} for DOPC/DOPE/SM/CH membranes. We showed by x-ray diffraction that this PEG concentration results in an intermembrane (phosphate-to-phosphate) distance of ~5 Å (54.6 Å lamellar repeat period in x-ray experiments minus 40 Å bilayer thickness minus 10 Å headgroup size) for DOPC/DOPE/SM/CH multilayers (10). The current result with a complex lipid mixture that fuses at very low PEG concentration strengthens the concept that a critical interbilayer distance is a requirement for fusion. However, the fact that a significant f_{LM} value occurs when f_{CM} is 0 means that significant outer-leaflet merger can occur even when conditions are still suboptimal for fusion pore formation.

CONCLUSIONS

There are several significant conclusions that stem from this work:

1. A sequential, two-intermediate model is both necessary and sufficient to describe PEG-mediated fusion of model membrane vesicles.
2. Analysis of time courses of PY-CH excimer/monomer fluorescence ratio and 90° light scattering (reversible events) support the assumption that fusion of PEG-aggregated vesicles is essentially irreversible. In other systems, this assumption might not hold and should be tested when interpreting experimental data from other systems.
3. Not all systems fuse via two intermediates. In some cases, only a single intermediate can be resolved and proceeds directly to a final pore, which has the properties of leakage and lipid mixing, just as I_2 has these properties for two-intermediate systems.
4. The ''states'' of membrane fusion defined by kinetic measurements are not well-defined structures as often shown in cartoons. Instead, a state is an ensemble of similar structures, the physical properties (content and lipid mixing, leakage) of which are described in terms of probabilities.
5. Two types of fusion pores are likely for PEG-mediated fusion, one associated with leakage and one being leakage free.

The kinetic model proposed here not only suggests interpretation of experimental observations but also provides the means of testing it. Kinetic analysis at multiple temperatures should reveal the activation energies of events in one- and two-intermediate systems that will help test our interpretation.

APPENDIX I

Here we present our derivation of expressions for a one-intermediate model similar to those given without derivation for the two-intermediate model in the ''Model development and computational procedures'' section of the text.

$$A \xrightarrow{k_1} I \xrightarrow{k_2} FP$$

Evolution of fusion states

This sequential model is described by a system of ordinary differential equations:

$$\begin{aligned} \frac{dA(t)}{dt} &= -A(t)k_1, \\ \frac{dI(t)}{dt} &= A(t)k_1 - I(t)k_2, \\ \frac{dFP(t)}{dt} &= I(t)k_2, \\ A(0) &= 1, I(0) = FP(0) = 0. \end{aligned} \tag{A1}$$

The solution of this set of equations is a superposition of exponents:

$$\begin{aligned} A(t) &= e^{-k_1 \times t}, \\ I(t) &= k_1 \frac{e^{-k_2 \times t} - e^{-k_1 \times t}}{k_1 - k_2}, \\ FP(t) &= -\frac{k_2}{k_1 - k_2}\left(1 - e^{-k_1 \times t}\right) + \frac{k_1}{k_1 - k_2}\left(1 - e^{-k_2 \times t}\right). \end{aligned} \tag{A2}$$

Observable events

The expressions for the observables (fluorescence of lipid mixing, content mixing, and leakage) are as follows:

Lipid mixing

$$\Phi_{LM}(t) = \beta_1 I(t) + FP(t), \Phi_{LM}(0) = 0. \tag{A3a}$$

Content mixing

$$\frac{d\Phi_{CM}(t)}{dt} = \alpha_1\frac{dI(t)}{dt} + (\alpha_1+\alpha_3)\frac{dFP(t)}{dt} - \Phi_{CM}(t)\times(A(t)\lambda_0 + I(t)\lambda_1), \qquad \Phi_{CM}(0) = 0. \tag{A3b}$$

Leakage

$$\frac{d\Phi_L(t)}{dt} = -\Phi_{CM}(t)^*(A(t)\lambda_0 + I(t)\lambda_1). \tag{A3c}$$

The expressions constraining and normalizing the probabilities are:

$$\alpha_0 = 0, \quad \beta_0 = 0, \quad \alpha_1+\alpha_3 = 1, \quad \beta_1+\beta_3 = 1. \tag{A4}$$

Solutions

And the analytical solutions for the Φ-values are:

LM

$$\Phi_{LM}(t) = \frac{k_1-\beta_1k_1}{k_1-k_2}\left(1-e^{-k_2\times t}\right) - \frac{k_2-\beta_1k_1}{k_1-k_2}\left(1-e^{-k_1\times t}\right), \tag{A5a}$$

Leakage

$$\Phi_L(t) = e^{-\lambda_0\frac{(1-e^{-k_1t})}{k_1}}e^{-\lambda_1\frac{-(1-e^{-k_1t})\times k_2+(1-e^{-k_2t})k_1}{k_2(k_1-k_2)}}. \tag{A5b}$$

The time evolution of content mixing could not be obtained analytically and was determined by the procedure outlined in Appendix II.

APPENDIX II

Eqs. 8b and A3b for content mixing could not be solved analytically. To avoid use of more complicated computer programming techniques, we used the following simplification. We found that the content mixing signal could always be described empirically by two exponentials:

$$\Phi_{CM}(t) = a\left(1-e^{-\nu_1\times t}\right) + b\left(1-e^{-\nu_2\times t}\right). \tag{B1}$$

This yielded arbitrary fitting parameters a, b, ν_1, and ν_2 that could not give us the content mixing parameters (α_i) we sought, but that allowed us to substitute an analytical expression for $\Phi_{CM}(t)$ in the second term of Eqs. 8b and A3b. As long as the effects of leakage on content mixing are small, this is a reasonable approximation. This allowed us to solve these equations analytically, and obtained another expression for Φ_{CM}, which now included the needed parameters:

$$\begin{aligned}\Phi_{CM}(t) = {} & \alpha_1 I(t) + (\alpha_1+\alpha_3)FP(t) \\ & - \left(\lambda_0 - \lambda_1\times\frac{k_1}{k_1-k_2}\right)\times\left[a\left(\frac{1-e^{-k_1\times t}}{k_1} - \frac{1-e^{-(k_1+\nu_1)\times t}}{k_1+\nu_1}\right) + b\left(\frac{1-e^{-k_1\times t}}{k_1} - \frac{1-e^{-(k_1+\nu_2)\times t}}{k_1+\nu_2}\right)\right] \\ & - \lambda_1\times\frac{k_1}{k_1-k_2}\times\left(a\left(\frac{1-e^{-k_2\times t}}{k_2} - \frac{1-e^{-(k_2+\nu_1)\times t}}{k_2+\nu_1}\right) + b\left(\frac{1-e^{-k_2\times t}}{k_2} - \frac{1-e^{-(k_2+\nu_2)\times t}}{k_2+\nu_2}\right)\right),\end{aligned} \tag{B2}$$

where a, b, ν_1, and ν_2 are obtained using Eq. B1. This equation was then used to globally fit the original content-mixing and leakage data by adjusting the α_i, λ_i, and k_i. Next, we checked this solution using the method of Runge-Kutta (35) to numerically solve differential Eq. A3b, where the α_i and k_i parameters were fixed at values found from fitting to Eq. B2. If the solution passed Runge-Kutta, it was accepted.

We thank Drs. Moses Dennison, Emdadul Haque, and Vladimir Malinin for allowing us to analyze their unpublished data and for many useful discussions of our analysis.

This work was supported by U.S. Public Health Service grant GM32707 to B.R.L.

REFERENCES

1. Chernomordik, L., M. M. Kozlov, and J. Zimmerberg. 1995. Lipids in biological membrane fusion. *J. Membr. Biol.* 146:1–14.
2. Markin, V. S., M. M. Kozlov, and V. L. Borovjagin. 1984. On the theory of membrane fusion. The stalk mechanism. *Gen. Physiol. Biophys.* 3:361–377.
3. Chernomordik, L., M. Kozlov, G. Melikyan, I. Agidor, V. Markin, and Y. Chizmadzhev. 1985. The shape of lipid molecules and monolayers membrane fusion. *Biochim. Biophys. Acta.* 812:643–655.
4. Siegel, D. P. 1993. Energetics of intermediates in membrane fusion: comparison of stalk and inverted micellar intermediate mechanisms. *Biophys. J.* 65:2124–2140.
5. Siegel, D. P. 1999. The modified stalk mechanism of lamellar/inverted phase transitions and its implications for membrane fusion. *Biophys. J.* 76:291–313.
6. Malinin, V. S., and B. R. Lentz. 2004. Energetics of vesicle fusion intermediates: comparison of calculations with observed effects of osmotic and curvature stresses. *Biophys. J.* 86:2951–2964.
7. Katsov, K., M. Muller, and M. Schick. 2004. Field theoretic study of bilayer membrane fusion. *I. Hemifusion Mechanism. Biophys. J.* 87: 3277–3290.
8. Lee, J., and B. R. Lentz. 1997. Evolution of lipidic structures during model membrane fusion and the relation of this process to cell membrane fusion. *Biochemistry.* 36:6251–6259.
9. Chanturiya, A., L. V. Chernomordik, and J. Zimmerberg. 1997. Flickering fusion pores comparable with initial exocytotic pores occur in protein-free phospholipid bilayers. *Proc. Natl. Acad. Sci. USA.* 94: 14423–14428.

10. Haque, M. E., T. J. McIntosh, and B. R. Lentz. 2001. Influence of lipid composition on physical properties and PEG-mediated fusion of curved and uncurved model membrane vesicles: ''nature's own'' fusogenic lipid bilayer. *Biochemistry*. 40:4340–4348.

11. Haque, M. E., and B. R. Lentz. 2004. Roles of curvature and hydrophobic interstice energy in fusion: studies of lipid perturbant effects. *Biochemistry*. 43:3507–3517.

12. Evans, K. O., and B. R. Lentz. 2002. Kinetics of lipid rearrangements during poly(ethylene glycol)-mediated fusion of highly curved unilamellar vesicles. *Biochemistry*. 41:1241–1249.

13. Dennison, S. M., N. Greenfield, J. Lenard, and B. R. Lentz. 2002. VSV transmembrane domain (TMD) peptide promotes PEG-mediated fusion of liposomes in a conformationally sensitive fashion. *Biochemistry*. 41: 14925–14934.

14. Chen, P. S., Jr., T. Y. Toribara, and H. Warner. 1956. Microdetermination of phosphorus. *Anal. Chem.* 28:1756–1758.

15. Schwenk, E., and N. T. Werthessen. 1952. Studies on the biosynthesis of cholesterol. III. Purification of C14-cholesterol from perfusion of livers and other organs. *Arch. Biochem. Biophys.* 40:334–341.

16. Lentz, B. R., G. F. McIntyre, D. J. Parks, J. C. Yates, and D. Massenburg. 1992. Bilayer curvature and certain amphipaths promote poly(ethylene glycol)-induced fusion of dipalmitoylphosphatidylcholine unilamellar vesicles. *Biochemistry*. 31:2643–2653.

17. Malinin, V. S., and B. R. Lentz. 2002. Pyrene cholesterol reports the transient appearance of nonlamellar intermediate structures during fusion of model membranes. *Biochemistry*. 41:5913–5919.

18. Malinin, V. S., P. Frederik, and B. R. Lentz. 2002. Osmotic and curvature stress affect PEG-induced fusion of lipid vesicles but not mixing of their lipids. *Biophys. J.* 82:2090–2100.

19. Massenburg, D., and B. R. Lentz. 1993. Poly(ethylene glycol)-induced fusion and rupture of dipalmitoylphosphatidylcholine large, unilamellar extruded vesicles. *Biochemistry*. 32:9172–9180.

20. Wilschut, J., N. Duzgunes, R. Fraley, and D. Papahadjopoulos. 1980. Studies on the mechanism of membrane fusion: kinetics of calcium ion induced fusion of phosphatidylserine vesicles followed by a new assay for mixing of aqueous vesicle contents. *Biochemistry*. 19:6011–6021.

21. Talbot, W. A., L. X. Zheng, and B. R. Lentz. 1997. Acyl chain unsaturation and vesicle curvature alter outer leaflet packing and promote poly(ethylene glycol)-mediated membrane fusion. *Biochemistry*. 36: 5827–5836.

22. Malinin, V. S., M. E. Haque, and B. R. Lentz. 2001. The rate of lipid transfer during fusion depends on the structure of fluorescent lipid probes: a new chain-labeled lipid transfer probe pair. *Biochemistry*. 40:8292–8299.

23. Lentz, B. R., W. Talbot, J. Lee, and L. X. Zheng. 1997. Transbilayer lipid redistribution accompanies poly(ethylene glycol) treatment of model membranes but is not induced by fusion. *Biochemistry*. 36:2076–2083.

24. Burgess, S. W., T. J. McIntosh, and B. R. Lentz. 1992. Modulation of poly(ethylene glycol)-induced fusion by membrane hydration: importance of interbilayer separation. *Biochemistry*. 31:2653–2661.

25. Wu, J. R., and B. R. Lentz. 1991. Mechanism of poly(ethylene glycol)-induced lipid transfer between phosphatidylcholine large unilamellar vesicles: a fluorescent probe study. *Biochemistry*. 30:6780–6787.

26. Wu, J. R., and B. R. Lentz. 1994. A method for quantitative interpretation of fluorescence detection of poly(ethylene glycol)-mediated 1-palmitoyl-2-[[[2-[4-(phenyl-*trans*-1,3,5-hexatrienly)phenyl]ethyl] oxyl]carbonyl]3-*sn*-phosphatidylcholine (DPHpPC) transfer and fusion between phospholipid vesicles in the dehydrated state. *J. Fluoresc.* 4: 153–163.

27. Kozlov, M. M., S. L. Leikin, L. V. Chernomordik, V. S. Markin, and Y. A. Chizmadzhev. 1989. Stalk mechanism of vesicle fusion. Intermixing of aqueous contents. *Eur. Biophys. J.* 17:121–129.

28. Spruce, A. E., L. J. Breckenridge, A. K. Lee, and W. Almers. 1990. Properties of the fusion pore that forms during exocytosis of a mast cell secretory vesicle. *Neuron*. 4:643–654.

29. Spruce, A. E., A. Iwata, J. M. White, and W. Almers. 1989. Patch clamp studies of single cell-fusion events mediated by a viral fusion protein. *Nature*. 342:555–558.

30. Chow, R. H., L. von Ruden, and E. Neher. 1992. Delay in vesicle fusion revealed by electrochemical monitoring of single secretory events in adrenal chromaffin cells. *Nature*. 356:60–63.

31. Alvarez de Toledo, G., R. Fernandez-Chacon, and J. M. Fernandez. 1993. Release of secretory products during transient vesicle fusion. *Nature*. 363:554–558.

32. Oberhauser, A. F., J. R. Monck, and J. M. Fernandez. 1992. Events leading to the opening and closing of the exocytotic fusion pore have markedly different temperature dependencies. Kinetic analysis of single fusion events in patch-clamped mouse mast cells. *Biophys. J.* 61: 800–809.

33. Clague, M. J., C. Schoch, L. Zech, and R. Blumenthal. 1990. Gating kinetics of pH-activated membrane fusion of vesicular stomatitis virus with cells: stopped-flow measurements by dequenching of octadecylrhodamine fluorescence. *Biochemistry*. 29:1303–1308.

34. Lee, J., and B. R. Lentz. 1998. Secretory and viral fusion may share mechanistic events with fusion between curved lipid bilayers. *Proc. Natl. Acad. Sci. USA*. 95:9274–9279.

35. Press, W. H., S. A. Teukolsky, W. T. Vetterling, and B. P. Flannery. 2002. Numerical Recipes in C++: The Art of Scientific Computing. Cambridge University Press.

36. Dennison, S. M., M. E. Bowen, A. T. Brunger, and B. Lentz. 2006. Neuronal snares do not trigger fusion between synthetic membranes but do promote PEG-mediated membrane fusion. *Biophys. J.* 90:1661–1675.

37. Yang, L., and H. W. Huang. 2002. Observation of a membrane fusion intermediate structure. *Science*. 297:1877–1879.

38. Muller, M., K. Katsov, and M. Schick. 2003. A new mechanism of model membrane fusion determined from Monte Carlo simulation. *Biophys. J.* 85:1611–1623.

39. Chanturiya, A., E. Leikina, J. Zimmerberg, and L. V. Chernomordik. 1999. Short-chain alcohols promote an early stage of membrane hemifusion. *Biophys. J.* 77:2035–2045.